



HAL
open science

Prediction of combustion noise of an enclosed flame by simultaneous identification of noise source and flame dynamics

Malte Merk, R Gaudron, Camilo Silva, Marco Gatti, Clément Mirat, Thierry Schuller, Wolfgang Polifke

► To cite this version:

Malte Merk, R Gaudron, Camilo Silva, Marco Gatti, Clément Mirat, et al.. Prediction of combustion noise of an enclosed flame by simultaneous identification of noise source and flame dynamics. Proceedings of the Combustion Institute, 2018, 37 (4), pp.5263-5270. 10.1016/j.proci.2018.05.124 . hal-02135730

HAL Id: hal-02135730

<https://hal.science/hal-02135730>

Submitted on 21 May 2019

HAL is a multi-disciplinary open access archive for the deposit and dissemination of scientific research documents, whether they are published or not. The documents may come from teaching and research institutions in France or abroad, or from public or private research centers.

L'archive ouverte pluridisciplinaire **HAL**, est destinée au dépôt et à la diffusion de documents scientifiques de niveau recherche, publiés ou non, émanant des établissements d'enseignement et de recherche français ou étrangers, des laboratoires publics ou privés.




Open Archive Toulouse Archive Ouverte (OATAO)

OATAO is an open access repository that collects the work of some Toulouse researchers and makes it freely available over the web where possible.

This is an author's version published in: <https://oatao.univ-toulouse.fr/23418>

Official URL : <https://doi.org/10.1016/j.proci.2018.05.124>

To cite this version :

Merk, Malte and Gaudron, Renaud and Silva, Camilo and Gatti, Marco and Mirat, Clément and Schuller, Thierry  and Polifke, Wolfgang *Prediction of combustion noise of an enclosed flame by simultaneous identification of noise source and flame dynamics*. (2018) Proceedings of the Combustion Institute, 37 (4). 5263-5270. ISSN 1540-7489

Any correspondence concerning this service should be sent to the repository administrator:

tech-oatao@listes-diff.inp-toulouse.fr

Prediction of combustion noise of an enclosed flame by simultaneous identification of noise source and flame dynamics

M. Merk ^{a, *}, R. Gaudron ^b, C. Silva ^a, M. Gatti ^b, C. Mirat ^b, T. Schuller ^{b, c},
W. Polifke ^a

^a *Fakultät für Maschinenwesen, Technische Universität München, Boltzmannstr. 15, Garching D-85747, Germany*

^b *Laboratoire EM2C, CNRS, CentraleSupélec, Université Paris-Saclay, 3, rue Joliot Curie, Gif-sur-Yvette cedex 91192, France*

^c *Institut de Mécanique des Fluides de Toulouse, IMFT, Université de Toulouse, CNRS, Toulouse, France*

Abstract

Large-Eddy Simulation (LES) is combined with advanced System Identification (SI) to simultaneously infer models for the source of combustion noise and the dynamic response to velocity fluctuations of a turbulent premixed flame. A Box-Jenkins model structure allows SI of both the noise source and the flame dynamics from time series data generated with single LES. The models that result from this ‘black-box’ SI approach are purely data-driven and do not rely on estimates of characteristic flow or flame parameters, such as turbulence intensity or flame length. In confined combustion systems the spectral distribution of combustion noise is strongly modulated by the cavity acoustics and the flame dynamics. By incorporating the identified models into a network model for the combustor acoustics, a linear Reduced Order Model (ROM) is built to predict the spectral distribution of sound pressure within the combustor for two different outlet reflection conditions. The identified flame transfer function as well as the ROM-based predictions of the pressure spectra in the combustor are compared with satisfactory qualitative and quantitative agreement against measurements. An interpretation of the pressure spectra based on eigenmode analysis elucidates the interplay between combustion noise generation, flame dynamics and cavity resonances.

Keywords: Combustion noise; Large-Eddy Simulation; System identification; Linear acoustic network model

1. Introduction

Combustion noise is an unavoidable by-product of turbulent combustion. For aeronautical engines it constitutes a significant contribution to the overall noise emissions [1]. Combustion noise re-

* Corresponding author.

E-mail address: merk@tfd.mw.tum.de (M. Merk).

URL: <http://www.tfd.mw.tum.de> (M. Merk)

sults from unsteady heat release by the flame [2]. The fluctuations of heat release rate may be seen as the sum of two contributions

$$\dot{Q}' = \dot{Q}'_c + \dot{Q}'_s. \quad (1)$$

Following the nomenclature of [3], \dot{Q}'_c denotes perturbations of heat release rate that result from acoustic velocity fluctuations upstream of the flame. This flame dynamic response may be taken into account via a Flame Transfer Function (FTF). Flame dynamics play a key role in self-excited thermoacoustic instability – which is not discussed further in the present paper – but can also shape the spectrum of combustion noise, as will be shown in the following. The second term \dot{Q}'_s describes a broadband *source of combustion noise*, which results from stochastic activity of the turbulent flow field and is understood to be uncorrelated with incoming acoustic perturbations.

Regarding the spectral distribution of noise generated by turbulent flames, one should distinguish between unconfined and enclosed configurations. In unconfined configurations, the sound pressure spectrum strongly correlates with \dot{Q}'_s and is thus of broadband nature. Nevertheless, even in this case \dot{Q}'_c cannot be neglected: flame intrinsic thermoacoustic (ITA) feedback may establish a two-way coupling between flame and acoustics [3,4], where the acoustic field generated by the flame causes velocity fluctuations upstream of the flame. These fluctuations in turn perturb the flame, causing a contribution \dot{Q}'_c to the fluctuations of heat release rate that may go in constructive or destructive interference with the noise source term \dot{Q}'_s . Consequently, the sound pressure spectrum is modulated. In case of an enclosed flame, acoustic reflections at the system boundaries constitute an additional feedback loop, which may modulate the shape of the sound pressure spectrum in a distinctive manner. The noise source \dot{Q}'_s may excite an acoustic cavity mode, causing resonance peaks in the pressure spectrum [3,4]. Hence, the sound pressure level and its spectral distribution depend in general strongly on the acoustic boundaries of the combustion system [5,6].

To reduce the overall sound pressure level in applied confined systems and to better understand the nature of the sound spectrum, accurate, reliable and flexible prediction methods are necessary, which take all relevant thermo-acoustic mechanisms into account. ‘Flexible’ here means that it should be possible to assess in a convenient and affordable manner the effect of changes in the acoustic boundary conditions, say, or the combustor geometry on the pressure spectrum.

Obviously, sound pressure levels in a combustion system may be determined by measurement [6–8]. However, experiments are rather laborious and inflexible in regard to changes in the acous-

tic boundaries. Reactive compressible Large-Eddy Simulation (LES) resolves directly the combustion noise generation as well as the acoustic propagation and reflection within the cavity and has proven itself to be capable of reproducing accurately the sound pressure spectra in confined systems [8–10]. Even though changes in the acoustic boundaries are feasible to implement, the computational effort of LES is considerable, and the investigation of a wide range of parameters, say, is prohibitively expensive.

Linear acoustic network models, on the other hand, are computationally much less demanding. Acoustic propagation, reflection and dissipation are described by network elements that relate the acoustic field up- and downstream of each element. In combination with an FTF, which describes the flame dynamics, and a model for the generation of combustion noise, a Reduced Order Model (ROM) can be formulated that should allow quantitative estimation of the sound pressure level for thermoacoustically stable configurations [3,4]. Whereas acoustic propagation, damping and reflection within the network model are rather straightforward to describe, the determination of the FTF and the noise source is more challenging.

A combustion noise source vector in terms of emitted characteristic wave amplitudes may be extracted experimentally [4,11], but the experimental assessment of the combustion noise source is difficult and laborious. An alternative approach relies on a Strouhal number scaling for the noise source [12–14]. These models predict an increase of the combustion noise source strength towards a peak frequency, with a subsequent roll-off to higher frequencies. These estimations rely on various assumptions that depend on the flame type and require detailed information about the flow field and the flame shape as model input.

The reader is reminded at this point that according to Eq. (1) the determination of only the noise source \dot{Q}'_s is not sufficient for an accurate prediction of combustion generated sound via a ROM. The possibility of two-way coupling requires to take into account also the flame response to acoustic fluctuations \dot{Q}'_c , i.e. to incorporate also the FTF into the ROM [3,4].

In the current work the FTF as well as a noise source model are derived from a LES / System Identification (LES/SI) approach [15]. Instead of the widely used Finite Impulse Response (FIR) identification [16,17], which only estimates the FTF from broadband LES time series data, a Box-Jenkins (BJ) model identification is applied [18]. In addition to a deterministic part, the BJ model includes also the estimation of a stochastic process. This model structure corresponds directly to the two contributions of the heat release fluctuations shown in Eq. (1) and makes possible the simultaneous identification of the FTF *and* the noise source from

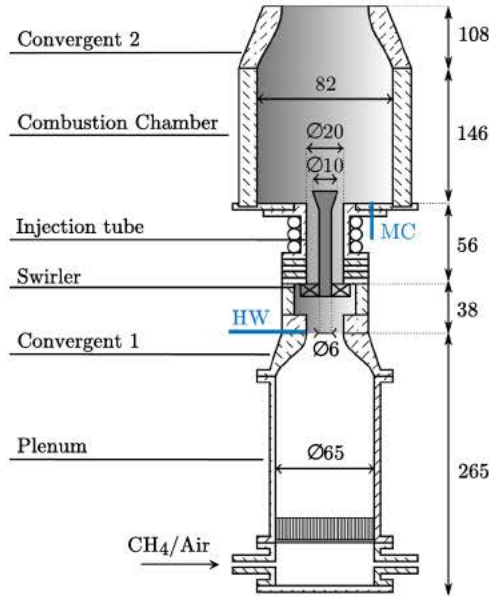


Fig. 1. Experimental setup of the turbulent swirl combustor. The shaded area represents the part of the test rig resolved within the LES. Dimensions are given in mm.

a single broadband LES time series data set. The black-box identification provides a purely data-driven noise model.

Application of BJ identification in the field of thermoacoustics was explored by Silva et al. [19] in a numerical study of a laminar flame, where stochastic combustion noise was mimicked by imposed equivalence ratio fluctuations. Merk et al. [18] investigated on the basis of surrogate data the general applicability of BJ identification to thermoacoustic systems, with emphasis on optimal model order, error margins and confidence levels. The present study is the first to apply BJ identification to actual LES time series data of a turbulent combustor and to juxtapose the subsequent ROM-based predictions of sound pressure spectra with a unique set of experimental results, where the flame dynamics (i.e. the FTF), the spectral distribution of sound pressure and the acoustic boundary conditions were measured with quantitative accuracy.

2. Experimental configuration

The turbulent swirl combustor shown in Fig. 1 was developed at EM2C laboratory, Paris. A methane and air mixture of equivalence ratio equal to $\phi = 0.82$ is injected at the bottom of the plenum. After flowing through the upstream plenum, a first convergent (contraction ratio: 8.73), a radial swirler and an injection tube, the mixture enters the combustion chamber. In the injection tube of diameter $D = 20$ mm, which has a reduced cross section due

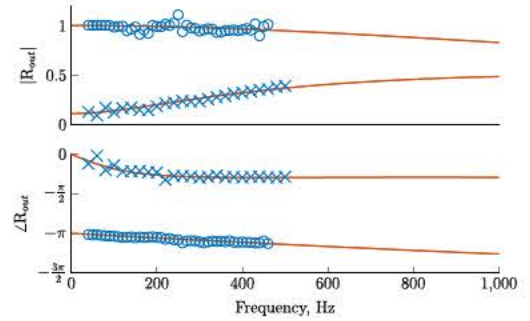


Fig. 2. Measured modulus (top) and phase (bottom) of the outlet reflection coefficients for an open end (o) and a perforated plate (x). Solid lines (—) show the fitted transfer functions used in the ROM.

to the central bluff body, a bulk flow velocity of $u_b = 7.1$ m/s is reached yielding a Reynolds number of $Re = u_b D / \nu \approx 7000$ at $p = 1$ atm and $T = 20^\circ\text{C}$. In the combustion chamber a swirl stabilized V-shaped flame develops with a thermal power of $P_{th} = 5.5$ kW. The burnt gases leave the combustion chamber through a small convergent exhaust (contraction ratio: 2.03) without indirect combustion noise production.

In order to measure the FTF, acoustic forcing is applied with a loudspeaker (Monacor SP-6/108PRO - 100 W RMS) mounted at the plenum bottom. At the reference position “HW” in Fig. 1, the resulting velocity fluctuations u'_{ref} are measured by a hot-wire probe (Dantec Dynamics Mini-CTA 54T30 with a 55P16 probe). Combustion chamber walls made of quartz glass provide optical access to the flame. A photomultiplier mounted with an interferometric filter centered on 310 ± 10 nm records the OH^* chemiluminescence signal of the flame, which is assumed to be proportional to the heat release rate. The FTF is deduced from the photomultiplier and hot-wire signals by sweeping the excitation frequency while maintaining a perturbation level of 10% of the mean flow speed at the hot wire probe.

The acoustic pressure within the combustion chamber is measured by the microphone “MC” in Fig. 1. It is mounted on a water-cooled waveguide, which is connected to the backplate of the combustion chamber. A fully reflecting rigid wall terminates the upstream end of the combustor. On the downstream side the combustor is either open-ended or equipped with a perforated plate having the same outer diameter as the convergent exhaust and a square pattern of 12 holes of radius $R = 2.5$ mm with an inter-hole spacing $d = 20$ mm. For both conditions, the reflection coefficient is measured with the three-microphone method [20]. Results are shown in Fig. 2. Uncertainties in the measurement of the pressure fluctuation (and thus in the measurement of the reflection coefficient) arise

in the vicinity of pressure nodes. These uncertainties are reduced using a switching method during data acquisition and coherence functions during data post-processing.

3. Simultaneous identification of Flame Transfer Function and noise model from LES

To determine the FTF and the noise source numerically, the time series data of a compressible LES is post-processed via advanced SI techniques. Flame dynamics, noise generation and acoustic propagation are all accounted for in the compressible LES by means of the solver AVBP [21]. The LES domain, represented by the shaded area in Fig. 1, fully resolves the radial swirler and the combustor geometry without geometric simplifications. An unstructured mesh with approximately 19 million tetrahedral cells exhibits a maximum cell size of 0.6 mm in the flame region and 1.5 mm the burnt gas region, respectively. A dynamically thickened flame model [22] resolves the flame thickness with at least 7 cells. A global 2-step chemical reaction mechanism optimized for premixed methane/air mixture is used [23]. Non-reflective boundary conditions using a wave masking technique [24] are applied. The upstream plenum is not part of the LES domain. From experiments, however, it is known that the flow after the first convergent is laminar. Thus, a laminar velocity profile is imposed at the inlet. For further details and validation of the LES setup, the reader is referred to [8].

Instead of deducing laboriously the flame response at discrete frequencies from repeated LES runs with harmonic flow forcing, a broadband excitation signal is applied at the LES inlet. The wavelet type excitation signal used has a constant power spectral density up to a cut-off frequency of 1000 Hz. As in experiment the forcing amplitude corresponds to 10% of the mean inlet velocity. Note that a trade-off has to be made, regarding the forcing amplitude. A small forcing amplitude yields a low signal-to-noise ratio with possibly unsatisfactory results of the identification procedure [18]. A large forcing amplitude may trigger a non-linear flame response, which can not be adequately described by the linear identification techniques used. Time series data of the acoustic velocity fluctuations at the reference position $u'_{\text{ref}}(t)$ (input) and of the total heat release rate fluctuations $\dot{Q}'(t)$ (output) are extracted from the LES. The length of the generated input-output time series amounts to 350 ms, which is down sampled to a cut-off frequency of 1000 Hz for the subsequent BJ identification.

As shown in Eq. (1) the key concept is to separate the fluctuations of total heat release rate into two contributions: a part resulting from the acoustic excitation \dot{Q}'_c , and a second term \dot{Q}'_s that is un-

correlated to the acoustic forcing, but instead accounts for the contribution of combustion noise. By definition, a BJ model is composed of a deterministic sub-model plus a sub-model for stochastic noise – a structure that corresponds exactly to the modeling approach implied by Eq. (1). Formally, one writes

$$\dot{Q}'(t, \theta) = \underbrace{\frac{B(q, \theta)}{F(q, \theta)} u'_{\text{ref}}(t)}_G + \underbrace{\frac{C(q, \theta)}{D(q, \theta)} e(t)}_H. \quad (2)$$

The deterministic model G represents the FTF and establishes a causal relation between the input $u'_{\text{ref}}(t)$ and the deterministic part of the output $\dot{Q}'(t, \theta)$. Conversely, the noise model H filters a Gaussian White Noise input signal $e(t)$, which is *uncorrelated* to the input signal.

The filters $B(q, \theta)$, $F(q, \theta)$ and $C(q, \theta)$, $D(q, \theta)$ that appear in the above equation are polynomials in the time shift operator q , defined as $q^{-i} u'_{\text{ref}}(t) \equiv u'_{\text{ref}}(t - i\Delta t)$. The filters B and C relate prior inputs to the current output $\dot{Q}'(t, \theta)$. F and D can describe possible auto-regressive behavior, as they relate prior *outputs* $q^{-i} \dot{Q}'(t)$ to the current output. The vector of polynomial coefficients $\theta = \{b_0 \dots b_{n_b}, f_0, \dots, d_{n_d}\}$ weighs the relations between present as well as prior input and output signals. The number of prior samples taken into account is determined by the polynomial filter orders $\{n_b, n_c, n_d, n_f\}$. This becomes apparent when rewriting the above equation as follows

$$\dot{Q}'(t, \theta) = \underbrace{\sum_{i=0}^{n_b} b_i q^{-i} u'_{\text{ref}}(t)}_{\dot{Q}'_c} + \underbrace{\sum_{i=0}^{n_c} c_i q^{-i} e(t)}_{\dot{Q}'_s}. \quad (3)$$

This equation also makes explicit the structural equivalence of the BJ model to Eq. (1). During identification of a BJ model, the vector of polynomial model coefficients θ is estimated by a non-linear least-squares problem that minimizes the error between estimated and actual output [18].

To summarize, the model output $\dot{Q}'(t, \theta)$ results from a convolution of the respective polynomial filters with prior input and output samples, see Eq. (3). Note that if the polynomial filters F , C and D are set to unity, the widely used FIR model structure [16,17] is recovered. The FIR describes the combustion noise problem in a less comprehensive manner than the BJ model structure. Although combustion noise is known to be colored [25], the FIR approach does not identify a noise model, but instead treats the noise contribution as a white noise disturbance. The BJ identification, however, drops the white noise assumption by explicitly filtering a generic Gaussian White Noise signal $e(t)$ through the estimated noise filter H resulting in a

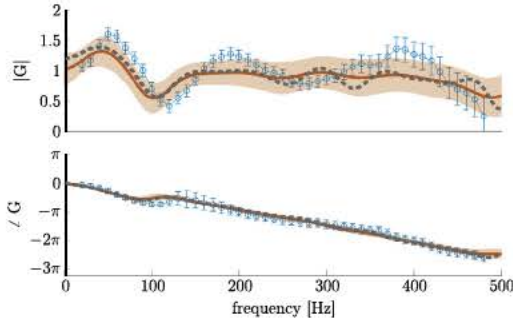


Fig. 3. Measured FTF values (\circ) with respective error bars. FTF identified via BJ identification (—) and via FIR identification (---). The shaded areas represent the 95% confidence interval of the FTF from the BJ model identification.

colored noise sub-model for $\dot{Q}_s(t, \theta)$. This contribution mimics directly the effect of colored turbulent velocity fluctuations that would cause a certain spectral distribution of heat release rate fluctuations, by shaping the same stochastic contribution from the generic Gaussian White Noise signal. Further details on the BJ model and its implications in the field of thermoacoustics can be found in [18].

By applying the BJ identification on the LES time series, the FTF (G) and the noise model (H) are identified simultaneously. Auto-regressive behavior within the FTF is not expected, thus n_f is set equal to $n_f = 1$. The remaining polynomial orders are set to $n_b = 30$, $n_c = 6$, $n_d = 6$. The data processing and the model identification are realized via MATLAB 2016b.

In Fig. 3 the identified FTF (—) is shown and compared against measured values (\circ). Error bars for the measured FTF values stem from three experimental data sets for the same operating conditions and represent reproducibility of the experiment. For further comparison the FTF is also identified with the established FIR model structure (---), in which the model order is chosen as the sum of $n_b + n_c + n_d$. The number of estimated parameters is hence equal in both approaches. For the FTF gain both identified models yield similar values and describe the measured FTF values with slight deviations. The phase values of the identified models are in excellent agreement with the measured values. Comparable results between BJ and FIR identification suggest that deviations from experimental results stem not from the BJ identification procedure. Rather uncertainties in the experimental measurement itself (see increasing error bars for increasing frequencies in Fig. 3) or inadequacies in the LES for the flame dynamics description might be responsible for the deviations.

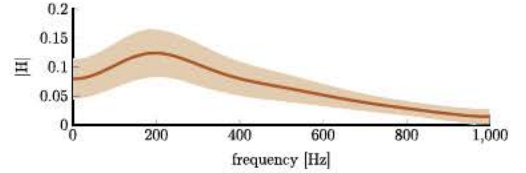


Fig. 4. Noise model identified via BJ identification (—) with 95% confidence interval represented by the shaded area.

Figure 4 depicts the identified noise model H . It shows that the noise source peaks slightly above 200 Hz. The amplitude of H has to be interpreted in terms of normalized heat release rate fluctuations, meaning that e.g. at 200 Hz, the noise source amplitude amounts to about 13% of the mean heat release rate. For the further usage of the noise model, the absolute level of noise fluctuations is consequently fixed by specifying the mean heat release rate.

As the BJ identification results in a data-driven model, a prerequisite for a reliable noise model identification is that the LES, from which the time series data is extracted, correctly reproduces the combustion noise generation. If the SI procedure is fed with erroneous data (e.g. if the LES generates spurious heat release rate fluctuations), erroneous noise models will result, independent of the chosen model structure. For the current study the validity of the LES with respect to the combustion noise generation was validated in [8] by comparing LES results against measured sound pressure spectra. Note that to a certain extent the combustion noise generation is independent from the flame dynamics. The generation of combustion noise strongly depends on the incoming turbulent velocity field, which in turn only plays a secondary role for the flame dynamics. This means that inaccuracies in the FTF identification are not directly transferable to the estimated noise model.

In closing this section it is remarked that the BJ identification could be applied to any signal in particular experimentally measured broadband data. However, since broadband forcing is not available in the test-rig facility, a one-to-one validation of the identified noise source model H for the combustion noise source is not possible. Nonetheless, the comparison presented below of measured and predicted sound pressure spectra, where the latter directly depends on the identified noise model H , corroborate the accuracy of the noise model H .

4. Reduced order model

The identified FTF and the noise model are incorporated into a linear acoustic network model of the combustor. The network model, which is

Table 1
Geometric and thermodynamic parameters of the ROM.

Plenum (p)	$R_{\text{in}} = 1$, $l_p = 0.265$ m, $A_p = 0.0033$ m ² $T_c = 300$ K, $\rho_c = 1.205$ kg/m ³
swirler (sw) + inj. tube	$l_{\text{sw}} = 0.06$ m, $l_{\text{inj}} = 0.034$ m, $A_{\text{inj}} = 3.5 \times 10^{-4}$ m ² , $\bar{u}_{\text{inj}} = 7.1$ m/s
comb. chamber (cc)	$l_{\text{cc}} = 0.146$ m, $A_{\text{cc}} = 6.7e-04$ m ² , $\Theta = 5.82$, $T_h = 1500$ K, $\rho_h = 0.235$ kg/m ³
convergent (conv.)	$R_{\text{out}}(\omega) = \text{see Fig. 2}$, $l_{\text{conv}} = 0.108$ m, $A_{\text{conv}} = 0.0033$ m ²

formulated in terms of the characteristic waves $f = 0.5 \cdot (p'/\bar{\rho}\bar{c} + u')$ and $g = 0.5 \cdot (p'/\bar{\rho}\bar{c} - u')$, is implemented in the open-source software taX [26]. The expressions for duct sections and area jumps, which are derived from linearized Euler equations, are written in terms of length and cross section ratio, respectively. No loss coefficients are introduced in order to avoid uncertain modeling parameters. For a detailed formulation of these elements the reader is referred to [3]. At the downstream end the reflection coefficient is taken into account by

$$\begin{bmatrix} f_d \\ g_d \end{bmatrix} = \begin{bmatrix} 0 & 0 \\ -R_{\text{out}}(\omega) & 1 \end{bmatrix} \begin{bmatrix} f_u \\ g_u \end{bmatrix} \quad (4)$$

Depending on the outlet condition studied, the outlet reflection coefficient R_{out} is adapted according to the polynomial fits shown in Fig. 2. At the combustor upstream end, the rigid plate is assumed to be fully reflecting with $R_{\text{in}} = 1$. The acoustic transfer behavior of the complex radial swirler geometry is represented by a 2×2 scattering matrix identified from LES on a domain that only comprises the swirler geometry. Note that the compressible LES takes acoustic losses across the swirler into account such that they are implicitly included in the identified scattering matrix of the radial swirler. Consequently, acoustic losses are only taken into account across the swirler element and at the downstream end via R_{out} . By means of the Rankine–Hugoniot jump conditions across a thin reaction zone [3,27], the identified FTF and the noise model are coupled into the linear network model across the flame element by

$$\begin{bmatrix} f_d \\ g_d \end{bmatrix} = \frac{1}{2} \begin{bmatrix} \xi + 1 & \xi - 1 \\ \xi - 1 & \xi + 1 \end{bmatrix} \begin{bmatrix} f_u \\ g_u \end{bmatrix} + \frac{1}{2} \frac{A_{\text{inj}}}{A_{\text{cc}}} \Theta G(\omega) \begin{bmatrix} 1 & -1 \\ -1 & 1 \end{bmatrix} \begin{bmatrix} f_{\text{ref}} \\ g_{\text{ref}} \end{bmatrix} - \mathbb{S}, \quad (5)$$

where the noise source \mathbb{S} is introduced as

$$\mathbb{S} = \frac{1}{2} \frac{A_{\text{inj}}}{A_{\text{cc}}} \bar{u}_{\text{inj}} \Theta H(\omega) e \begin{bmatrix} -1 \\ 1 \end{bmatrix} \quad (6)$$

Furthermore, ξ denotes the specific acoustic impedance and Θ the temperature jump across the flame $\Theta = T_b/T_c - 1$. The transfer matrix of the passive flame, i.e. the temperature discontinuity across the flame, is taken into account by the first term on the rhs. of Eq. (5). The second term

describes the active flame part and hence the effect of unsteady flame heat release in response to velocity perturbations at the reference position. The third term \mathbb{S} accounts for the contribution from the combustion noise source term. Note that this formulation implicitly recovers the two-way coupling between noise source and flame dynamics [3]. All parameters used in the network model are given in Table 1.

The eigenfrequencies predicted by the network model (\times) agree with measured eigenfrequencies for *non-reactive* conditions, see Fig. 6. The FTF is not taken into account here. Only the fourth eigenmode shows a slight discrepancy. Thus, it is concluded that the acoustic network model fairly well captures the eigenmodes of the combustor cavity, which is a prerequisite for the following sound pressure prediction of the reactive setup. Moreover, in Fig. 6 it gets evident that an increase of the mean temperature in the combustion chamber T_h mainly affects the second eigenmode. This eigenmode corresponds predominantly to a $\lambda/4$ wave mode within the combustion chamber. Hence, its frequency is strongly modulated by an increased combustion chamber temperature and the thereof resulting increase in the speed of sound. The first and third eigenmode are associated with the combustor Helmholtz mode and a $\lambda/2$ plenum mode, respectively. Both are predominantly active in the plenum and consequently hardly affected by the increase of T_h .

5. ROM based sound pressure predictions

The ROM, now including the identified FTF model $G(\omega)$ and the noise model $H(\omega)$, is evaluated in the frequency domain and the spectrum of the acoustic pressure fluctuations in the combustion chamber (p'_{MC} in Fig. 5) is compared with corresponding measurements. The 95% confidence interval is computed by propagating the uncertainties of the identified noise model through the network model. The influence of the uncertainties in the FTF identification on the sound pressure prediction are found to be small and are thus neglected.

Fig. 7 shows excellent agreement between the experimental spectrum ($\odot\odot\odot$) and the ROM prediction (—). Note that due to the cavity acoustics, the sound pressure spectrum differs markedly from the spectral distribution of the combustion

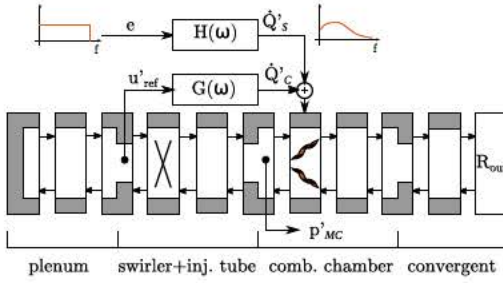


Fig. 5. Reduced order model used. The radial swirler part is replaced by a scattering matrix identified via LES/SI.

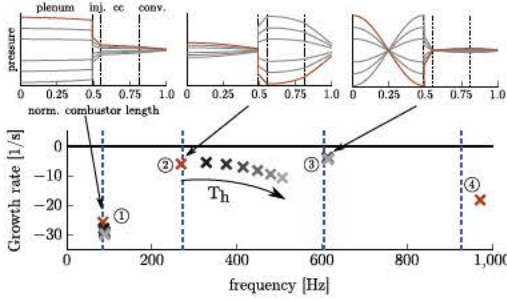


Fig. 6. Frequencies of the measured *cold* eigenmodes (— — —) and the *cold* eigenmodes predicted by the network model (×) for the open-ended configuration. Gray-scaled crosses represent the frequency shift if the mean temperature in the combustion chamber is increased up to $T_h = 1500$ K.

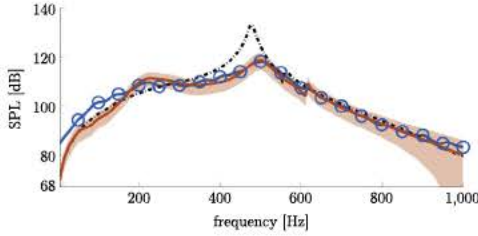


Fig. 7. Measured sound pressure spectrum (○○○) and ROM prediction for the open-ended configuration: two-way coupling (—) with confidence interval, one-way coupling (---).

noise source: the maximum in the combustion noise source spectrum near 200 Hz seen in Fig. 4 generates only a secondary peak in the sound pressure spectrum, which indeed has its maximum around 515 Hz. This peak arises from resonance with the second cavity mode – Fig. 6 shows that its eigenfrequency is somewhat above 500 Hz if the combustion chamber temperature T_h is increased.

The sound pressure spectrum predicted by the one-way coupling approach is also shown in Fig. 7 (---). The FTF is not taken into account

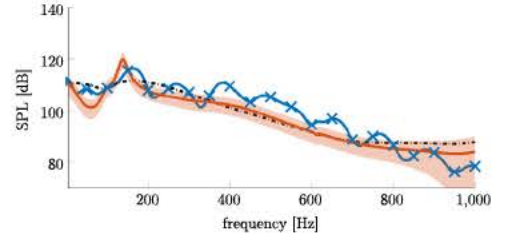


Fig. 8. Measured sound pressure spectrum (×××) and ROM prediction for the configuration equipped with a perforated plate: two-way coupling (—) with confidence interval, one-way coupling (---).

here, such that the cavity is only excited by the noise source. Hence, the feedback from the acoustic field onto the upstream velocity field and the thereof resulting heat release rate fluctuations are neglected. Overall, one-way coupling produces acceptable results, with the exception of amplitude and frequency of the spectral peak that results from acoustic resonance. Similar behavior is reported in [3]. Note that taking \dot{Q}_c into account, as it is done with two-way coupling (—), does not necessarily imply an increase in the sound pressure spectrum. The relative phase between \dot{Q}_s and \dot{Q}_c determines whether interference is constructive or destructive.

Figure 8 shows the sound pressure spectra that result if the downstream end of the combustor is equipped with the perforated plate. Note that jet noise generated by the flow crossing the perforated plate causes a less smooth experimental spectrum compared to the open-ended configuration shown in Fig. 7. From evaluating the mode shapes depicted in Fig. 6, it is evident that a change of the outlet reflection condition mainly affects the second cavity mode. Indeed, the sound pressure peak observed in the open-ended configuration vanishes when the combustor is terminated by the perforated plate. A decreased outlet reflection reduces acoustic reflections at the system boundary and consequently weakens the modulation of the sound pressure spectrum by the cavity acoustics. As a result the sound pressure spectrum follows more closely the spectral distribution of the combustion noise source shown in Fig. 4. Note that a change in the acoustic boundary of the combustor does neither modify the flame dynamics nor the combustion noise source. Thus, the same models for $G(\omega)$ and $H(\omega)$ are used and the experimental results can be reproduced with negligible computational cost by merely adjusting the cavity of the network model.

6. Conclusion

Models for the source of combustion noise and the flame dynamics are identified simultaneously from a single broadband LES time series by Box-Jenkins system identification. Compared to the

established finite impulse response, a Box-Jenkins structure estimates also a model for the noise characteristics, which constitutes a novelty in the field of thermoacoustics. The Box-Jenkins model does not assume white noise and allows thus the additional identification of a data-driven noise model, which provides insight into the amplitude and spectral distribution of the combustion noise source. Combined with a linear network model for the cavity acoustics of the combustor, a reduced order model is built to predict sound pressure spectra and their associated confidence intervals. Two different configurations are studied that differ by their respective outlet reflection coefficient. Since a change in the acoustic boundary does not affect the flame dynamics and the combustion noise source, only the outlet reflection coefficient of the reduced order model has to be adopted to represent the two configurations. Convincing agreement with measurements of flame transfer function and sound pressure spectra is found. Compared to stand-alone LES, the proposed methodology allows the evaluation of the sound pressure spectrum across a large parameter space with reduced computational effort. Even if the flame operating conditions change, only *one* additional LES computation is required to derive again models for the flame dynamics and the noise source. Although it would also be possible to directly extract the sound pressure level for *one* certain configuration from LES, the ROM approach provides additionally valuable insight into the interplay between generation of combustion noise, flame dynamics and cavity resonances. Hence, a computational efficient approach is retained that offers a comprehensive examination of the nature of sound pressure peaks and allows the optimization of the combustor in terms of combustion noise levels reached.

Acknowledgment

Financial support is acknowledged by the DFG (project PO 710/16-1), by the ANR (project ANR-14-CE35-0025-01) and by the European Union's Horizon 2020 research and innovation programme under the Marie Skłodowska-Curie grant agreement No 643134. Computing time on the GCS Supercomputer SuperMUC was provided by Gauss Centre for Supercomputing e.V.

References

- [1] A.P. Dowling, Y. Mahmoudi, *Proc. Combust. Inst.* 35 (1) (2015) 65–100, doi:10.1016/j.proci.2014.08.016.
- [2] W.C. Strahle, *Prog. Energy Combust. Sci.* 4 (1978) 157–176, doi:10.1016/0360-1285(78)90002-3.
- [3] C.F. Silva, M. Merk, T. Komarek, W. Polifke, *Combust. Flame* 182 (2017) 269–278, doi:10.1016/j.combustflame.2017.04.015.
- [4] B.B.H. Schuermans, W. Polifke, C.O. Paschereit, J.H. van der Linden, in: *ASME 2000-GT-105*, Munich, Germany, 2000.
- [5] N. Tran, S. Ducruix, T. Schuller, *Proc. Combust. Inst.* 32 (2) (2009) 2917–2924, doi:10.1016/j.proci.2008.06.123.
- [6] A. Lamraoui, F. Richecoeur, T. Schuller, S. Ducruix, *J. Eng. Gas Turbines Power* 133 (1) (2011) 011504, doi:10.1115/1.4001987.
- [7] V. Bellucci, B. Schuermans, D. Nowak, P. Flohr, C.O. Paschereit, *J. Turbomach.* 127 (2) (2005) 372–379, doi:10.1115/1.1791284.
- [8] M. Merk, R. Gaudron, M. Gatti, C. Mirat, T. Schuller, W. Polifke, *AIAA J.* (2018) 1–13, doi:10.2514/1.J056502.
- [9] M. Huet, F. Vuillot, N. Bertier, M. Mazur, N. Kings, W. Tao, P. Scoufflaire, F. Richecoeur, S. Ducruix, C. Lapeyre, T. Poinso, *J. AerospaceLab* (11) (2016), doi:10.12762/2016.AL11-10.
- [10] J.M. Lourier, M. Stöhr, B. Noll, S. Werner, A. Filolitakis, *Combust. Flame* 183 (2017) 343–357, doi:10.1016/j.combustflame.2017.02.024.
- [11] C.O. Paschereit, B.B.H. Schuermans, W. Polifke, O. Mattson, *J. Eng. Gas Turbines Power* 124 (2) (2002) 239–247, doi:10.1115/1.1383255.
- [12] C. Hirsch, J. Wäse, A. Winkler, T. Sattelmayer, *Proc. Combust. Inst.* 31 (1) (2007) 1435–1441, doi:10.1016/j.proci.2006.07.154.
- [13] R. Rajaram, T. Lieuwen, *J. Fluid Mech.* 637 (2009) 357–385, doi:10.1017/S0022112009990681.
- [14] Y. Liu, *J. Sound Vib.* 353 (2015) 119–134, doi:10.1016/j.jsv.2015.05.027.
- [15] W. Polifke, *Ann. Nucl. Energy* 67C (2014) 109–128, doi:10.1016/j.anucene.2013.10.037.
- [16] A. Giauque, T. Poinso, F. Nicoud, in: Fourteenth AIAA/CEAS Aeroacoustics Conference (Twenty-Ninth AIAA Aeroacoustics Conference), AIAA/CEAS, Vancouver, Canada, 2008, doi:10.2514/6.2008-2943.
- [17] A. Innocenti, A. Andreini, B. Facchini, *Energy Procedia* 82 (2015) 358–365, doi:10.1016/j.egypro.2015.11.803.
- [18] M. Merk, S. Jaensch, C. Silva, W. Polifke, *J. Sound Vib.* 422 (2018) 432–452, doi:10.1016/j.jsv.2018.02.040.
- [19] C.F. Silva, W. Polifke, J. O'Brien, M. Ihme, in: Summer Program, Center for Turbulence Research, Stanford University, Stanford, USA, 2014, p. 179.
- [20] J.Y. Chung, D.A. Blaser, *J. Acoust. Soc. Am.* 68 (3) (1980) 914–921, doi:10.1121/1.384779.
- [21] CERFACS, IMFT, The AVBP HandBook, <http://www.cerfacs.fr/avbp6x/>, 2008.
- [22] O. Colin, F. Ducros, D. Veynante, T. Poinso, *Phys. Fluids* 12 (7) (2000) 1843–1863, doi:10.1063/1.870436.
- [23] B. Franzelli, E. Riber, M. Sanjosé, T. Poinso, *Combust. Flame* 157 (7) (2010) 1364–1373, doi:10.1016/j.combustflame.2010.03.014.
- [24] W. Polifke, C. Wall, P. Moin, *J. Comp. Phys.* 213 (2006) 437–449, doi:10.1016/j.jcp.2005.08.016.
- [25] H.A. Hassan, *J. Fluid Mech.* 66 (03) (1974) 445, doi:10.1017/S0022112074000292.
- [26] T. Emmert, S. Jaensch, C. Svardi, W. Polifke, in: Seventh Forum Acusticum, DEGA, Krakow, 2014.
- [27] J.J. Keller, *AIAA J.* 33 (12) (1995) 2280–2287, doi:10.2514/3.12980.